Physica D ▮ (▮▮▮▮) ▮▮▮–▮▮▮

Contents lists available at SciVerse ScienceDirect

Physica D

journal homepage: www.elsevier.com/locate/physd

Networks of theta neurons with time-varying excitability: Macroscopic chaos, multistability, and final-state uncertainty

Paul So *, Tanushree B. Luke, Ernest Barreto

School of Physics, Astronomy, and Computational Sciences, George Mason University, Fairfax, VA 22030, USA
The Krasnow Institute for Advanced Study, George Mason University, Fairfax, VA 22030, USA

HIGHLIGHTS

- Derived exact asymptotic dynamics for time-varying networks of theta neurons.
- Network exhibited macroscopic chaos, quasiperiodicity, and multistability.
- Network exhibited fractal basin boundaries and final-state uncertainty.
- Escape and switching behaviors depend on both macroscopic and microscopic initial states.
- Ability to redirect such macroscopic states with an accessible global parameter.

ARTICLE INFO

Article history:
Available online xxxx

Keywords:
Theta neuron
Time-varying network
Kuramoto system
Macroscopic chaos
Quasiperiodicity
Final-state uncertainty

ABSTRACT

Using recently developed analytical techniques, we study the macroscopic dynamics of a large heterogeneous network of theta neurons in which the neurons' excitability parameter varies in time. We demonstrate that such periodic variation can lead to the emergence of macroscopic chaos, multistability, and final-state uncertainty in the collective behavior of the network. Finite-size network effects and rudimentary control via an accessible macroscopic network parameter is also investigated.

1. Introduction

Natural networks, especially biological ones, are never static. The strength of interaction between network elements typically varies in time, often in response to the activity of the elements themselves. This is especially true of neuronal networks in the brain, in which, it is generally believed, learning occurs when synapses are strengthened or weakened in a Hebbian manner. Similarly, the internal dynamics of network elements might change in time as well. For example, the excitability characteristics of neurons can change in response to neuromodulators (e.g., dopamine), local accumulation of extracellular potassium, or other transient changes in the neuronal environment.

Developing a general understanding of the macroscopic dynamics of such evolving networks is the subject of a very active area of research. Our goal in the present work is to use recently-developed analytical techniques, applicable to large populations of simple oscillators (e.g., Kuramoto systems), to examine the complexity that can arise in heterogeneous networks of idealized neurons. In particular, we consider populations of theta neurons in which the excitability parameters of the neurons vary in time. In previous work [1], we showed that adding such time modulation to the coupling in a bimodal Kuramoto system can lead to increased complexity at the macroscopic level.

A neuron at rest begins to spike as a constant injected current exceeds a threshold. Neurons are typically classified into two types based on this behavior [2–4]. Type-I neurons begin to spike at an arbitrarily low rate, whereas Type-II neurons spike at a non-zero rate as soon as the threshold is exceeded. Neurophysiologically, excitatory pyramidal neurons are often of Type-I, and fast-spiking inhibitory interneurons are often of Type-II [5,6].

Ermentrout and Kopell [7,3] showed that, near the firing threshold, Type-I neurons can be represented by a canonical phase model that features a saddle–node bifurcation on an invariant cycle, or a SNIC bifurcation. This model has come to be known as the theta neuron, and is given by

$$\dot{\theta} = (1 - \cos\theta) + (1 + \cos\theta)\eta, \tag{1}$$

* Corresponding author at: The Krasnow Institute for Advanced Study, George Mason University, Fairfax, VA 22030, USA. Tel.: +1 7039934377.
E-mail addresses: paso@gmu.edu (P. So), tluke@gmu.edu (T.B. Luke), ebarreto@gmu.edu (E. Barreto).
URLs: http://complex.gmu.edu/~paso (P. So), http://complex.gmu.edu/~ernie (E. Barreto).

0167-2789/$ – see front matter © 2013 Elsevier B.V. All rights reserved.
http://dx.doi.org/10.1016/j.physd.2013.04.009

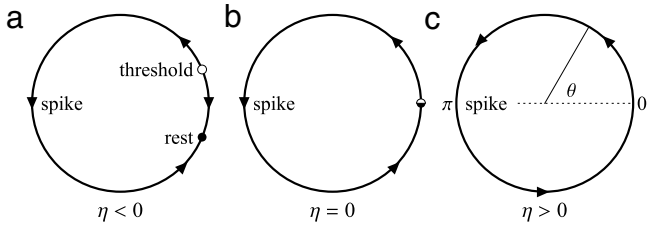

Fig. 1. The SNIC bifurcation of the theta neuron. (a) For $\eta < 0$, the neuron is excitable. (b) The SNIC bifurcation occurs for $\eta = 0$. (c) For $\eta > 0$, the neuron spikes regularly. Spikes occur when the phase variable θ crosses π, by definition.

where θ is a phase variable on the unit circle and η is a bifurcation parameter related to the injected current. The SNIC bifurcation occurs for $\eta = 0$. For $\eta < 0$, the neuron is attracted to a stable equilibrium which represents the resting state. An unstable equilibrium is also present, representing the threshold. If an external stimulus pushes the neuron's phase across the unstable equilibrium, θ will move around the circle and approach the resting equilibrium from the other side. When θ crosses $\theta = \pi$, the neuron is said to have spiked. Thus, for $\eta < 0$, the neuron is excitable.

As the parameter η increases, these equilibria merge in a saddle–node bifurcation and disappear, leaving a limit cycle. Consequently, the neuron spikes regularly. This transition is depicted schematically in Fig. 1.

If the theta neuron's excitability parameter η is made to oscillate sinusoidally, repeatedly crossing the SNIC bifurcation, the neuron becomes a parabolic burster [7], as shown in Fig. 2(a). Several biophysical mechanisms could modulate neuronal excitability in this manner. For example, synaptic barrages associated with characteristic brain rhythms create up and down states in cortical neurons [8]. Here, we take particular motivation from recent work in which the role of ion concentration dynamics in neuronal excitability was investigated [9,10]. In this work, a standard Hodgkin–Huxley neuron was augmented to permit the intra- and local extra-cellular concentrations of sodium and potassium to evolve dynamically. It was found that this extended model could undergo bifurcations to oscillatory states in which the ion concentrations vary periodically, driving the neuron into and out of its spiking regime, thus exhibiting periodic bursting.

It is well-known that the Hodgkin–Huxley neuron is a type-II neuron with respect to a constant injected current. However, the augmented Hodgkin–Huxley neuron described above is a Type-I neuron with respect to the local extracellular potassium. More precisely, if the ion concentrations are fixed, and the extracellular potassium concentration is treated as a bifurcation parameter for the neuron, the neuron transitions from resting to spiking via a SNIC bifurcation. An example of one such parabolic bursting behavior exhibited by this model is shown in Fig. 2(b). The dynamical mechanism underlying this behavior – crossing back and forth across a SNIC bifurcation – is identical to that of the theta neuron burster of Fig. 2(a). (See Ref. [9] for details.)

Based on all these considerations, we investigate in this paper the dynamics of a large heterogeneous network of coupled theta neurons in which the excitability parameters of the neurons are modulated in time. We analytically obtain the asymptotic mean field dynamics of such a network, and show that macroscopic chaos, multistability, and final-state uncertainty all occur. We also consider finite-size network effects, and show that these collective behaviors can be altered and directed by perturbing an accessible macroscopic parameter. Since the theta neuron is the canonical representation of Type-I neurons near their spiking thresholds, we expect that the complex macroscopic behaviors described in this study are generic features of any large network of Type-I neurons with time-varying excitability.

2. The model

2.1. Exact macroscopic dynamics of the reduced network

We consider a network of N theta neurons,

$$\dot{\theta}_j = \left(1 - \cos\theta_j\right) + \left(1 + \cos\theta_j\right)\left[\eta_j(t) + I_{syn}\right] \tag{2}$$

where $j = 1, \ldots, N$ is the index for the j-th neuron. The neurons are coupled via a pulse-like synaptic current I_{syn} by

$$I_{syn} = \frac{k}{N}\sum_{i}^{N} P_n(\theta_i) \tag{3}$$

where $P_n(\theta) = a_n\,(1 - \cos\theta)^n$, $n \in \mathbb{N}$ [11], and a_n is a normalization constant such that

$$\int_0^{2\pi} P_n(\theta)d\theta = 2\pi\,.$$

The parameter n defines the sharpness of the pulse-like synapse; it becomes more and more sharply peaked as n increases. The sum in Eq. (3) is over the entire population, and we assume that the synaptic strength k is the same for all neurons in the network.

Most importantly, we assume that each neuron's excitability parameter varies in time. This might occur, for example, via fluctuating ion concentrations, and in [9], it was found that the

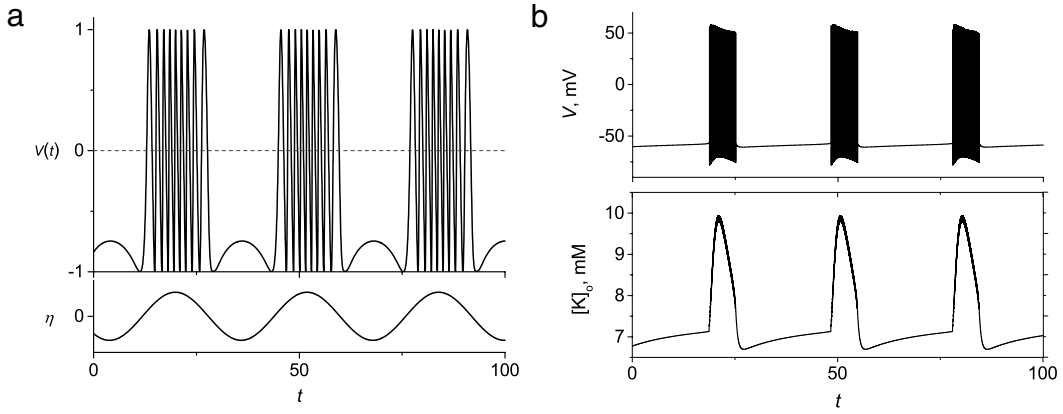

Fig. 2. Parabolic bursters. (a) Time trace of a voltage-like variable $V(t) = \sin(\theta)$ for a theta neuron with a time-varying excitability parameter $\eta(t) = \bar{\eta} + A\sin(2\pi t/\tau)$. The lower panel shows η versus time. (b) Voltage trace for the ion-concentration burster described in the text. The lower panel shows the local extracellular potassium concentration.

Please cite this article in press as: P. So, et al., Networks of theta neurons with time-varying excitability: Macroscopic chaos, multistability, and final-state uncertainty, Physica D (2013), http://dx.doi.org/10.1016/j.physd.2013.04.009

ion concentration dynamics typically settles onto a limit cycle. This observation, along with Ref. [7], motivated us to write

$$\eta_j(t) = \bar{\eta}_j + A\sin(2\pi(t+\delta_0)/\tau), \tag{4}$$

where $\bar{\eta}_j$ is the temporal mean of the excitability for the j-th neuron. A and τ are the same for all neurons and denote the magnitude and the period of the modulation, respectively, and we set $\delta_0 = 0$ unless we specify otherwise. We note that the reduction performed in the following section remains valid even if one replaces η_j as given in Eq. (4) by the solution of a differential equation of the form $\dot{\eta}_j = \Pi(\eta_j, z, t)$, where the function Π depends on η_j, a macroscopic mean field variable z (defined below), and time t.

In addition, since neurons in real biological networks exhibit a range of intrinsic excitabilities, we also assume that the median excitability $\bar{\eta}_j$ of each neuron is different. We model this network heterogeneity by assuming that each $\bar{\eta}_j$ is randomly drawn from a distribution $g(\bar{\eta})$. In the following analysis, we assume a Lorentzian distribution,

$$g(\bar{\eta}) = \frac{1}{\pi}\frac{\Delta}{(\bar{\eta}-\eta_0)^2+\Delta^2}, \tag{5}$$

where η_0 is the center of the distribution, and Δ, the half-width at half-maximum, describes the degree of heterogeneity in the population.

Following the mean-field approach pioneered by Kuramoto in 1975 [12] (and later used by many others [13]), we consider the limit $N \to \infty$ and move to a continuum description by introducing a probability density function $\rho(\theta, \bar{\eta}, t)$ that describes the distribution of neuronal oscillators. Specifically, the quantity $\rho(\theta, \bar{\eta}, t)d\theta d\bar{\eta}$ gives the fraction of neurons with phase in the range $[\theta, \theta+d\theta]$ and median excitability in $[\bar{\eta}, \bar{\eta}+d\bar{\eta}]$ at a particular time. Since the total number of neurons is conserved, ρ satisfies the following continuity equation:

$$\frac{\partial\rho}{\partial t} + \frac{\partial}{\partial\theta}(\rho v_\theta) = 0 \tag{6}$$

where the phase velocity v_θ is given by the continuum version of Eqs. (2) and (3),

$$v_\theta(\theta, \bar{\eta}, t) = (1-\cos\theta) + (1+\cos\theta) \times \left[\eta(t) + ka_n\int_{-\infty}^{\infty}\int_0^{2\pi}\rho(\theta', \bar{\eta}', t)(1-\cos\theta')^n d\theta' d\bar{\eta}'\right]. \tag{7}$$

Here, $\eta(t) = \bar{\eta} + A\sin(2\pi t/\tau)$.

The collective behavior of the infinite network can be described by a complex macroscopic mean-field variable $z(t)$ given by

$$z(t) = \int_{-\infty}^{\infty}\int_0^{2\pi}\rho(\theta, \bar{\eta}, t)e^{i\theta}\, d\theta d\bar{\eta}. \tag{8}$$

If one imagines the state of each individual neuron being represented by a phasor on the unit circle, the macroscopic mean field $z(t)$ gives the centroid of these phasors. Writing $z(t) = re^{i\phi}$, the magnitude r characterizes the degree of network coherence, and ϕ is the mean-field phase. Below, we derive a low-dimensional dynamical system whose asymptotic behavior exactly coincides with that of the infinite discrete network.

Our theta neuron network, Eqs. (2)–(3), can be written in *sinusoidally coupled* form [14], meaning that the individual oscillator's phase θ only appears via the harmonic functions $e^{i\theta}$ and $e^{-i\theta}$:

$$v_\theta = fe^{i\theta} + h + f^*e^{-i\theta} \tag{9}$$

where $*$ denotes complex conjugation,

$$f = -\frac{1}{2}\left[(1-\eta(t)) - kH(z,n)\right], \tag{10}$$

and

$$h = (1+\eta(t) + kH(z,n)). \tag{11}$$

Here, the rescaled synaptic current $H(z,n) = I_{syn}/k$ is written as a function of the mean-field variable z and the synapse sharpness parameter n, and is given by,

$$H(z,n) = a_n\left(C_0 + \sum_{q=1}^{n} C_q\left[z^q + (z^*)^q\right]\right) \tag{12}$$

with

$$C_q = \sum_{j,m=0}^{n}\delta_{j-2m,q}Q_{jm} \tag{13}$$

and

$$Q_{jm} = \frac{(-1)^j n!}{2^j m!(n-j)!(j-m)!}, \tag{14}$$

where $\delta_{i,j}$ is the standard Kronecker delta function on the indices (i,j). Further details are provided in Appendix A.

The sinusoidally coupled form of Eq. (9) defines a general class of globally-coupled phase oscillator networks which includes Josephson junction arrays and other Kuramoto-like systems. Stemming from its globally coupled nature, the functions f and h in general depend on the mean field z. While they cannot explicitly depend on the phase variable θ, they can be any sufficiently well-behaved functions with or without explicit dependence on time or other auxiliary dynamics. Here, we exploit this property by coupling the theta neuron network to the time-varying excitability parameter η that appears in f and h.

From the initial theoretical work by Watanabe and Strogatz on networks of identical Josephson junction arrays in the 1990s [15], to the recent resurgence of interest in other Kuramoto-like networks [16–20], developments in the analysis of collective dynamics of phase oscillator networks have produced a powerful set of new theoretical tools. These tools apply to our theta neuron network as well. Here, we follow the procedure of Ref. [16] and adopt the ansatz that the solution to the continuity equation, Eq. (6), can be written as a Fourier series

$$\rho(\theta, \bar{\eta}, t) = \frac{g(\bar{\eta})}{2\pi}\left\{1 + \sum_{q=1}^{\infty}(\alpha^*(\bar{\eta}, t)^q e^{iq\theta} + \alpha(\bar{\eta}, t)^q e^{-iq\theta})\right\} \tag{15}$$

in which $\alpha(\bar{\eta}, t)$ is a yet-to-be-determined complex function. In Eq. (15), the amplitudes in the Fourier expansion are monomials in α. This defines a two-dimensional subspace (parametrized by the real and imaginary parts of α) within the infinite-dimensional space of all possible probability density functions. In [16], Ott and Antonsen showed that this manifold (often called the OA or Poisson manifold) is attracting and invariant for the macroscopic dynamics if and only if α satisfies the differential equation

$$\dot{\alpha} = i(f\alpha^2 + h\alpha + f^*) \tag{16}$$

and $|\alpha(\bar{\eta}, t)| < 1$ for all time.

The macroscopic mean field is obtained by substituting Eq. (15) into Eq. (8), resulting in

$$z(t) = \int_{-\infty}^{\infty}\alpha(\bar{\eta}, t)g(\bar{\eta})d\bar{\eta}. \tag{17}$$

To evaluate this integral, $\alpha(\bar{\eta}, t)$ is analytically continued into the upper half of the complex $\bar{\eta}$-plane. With the Lorentzian in Eq. (5), the resulting contour integral can be evaluated in closed form in terms of the residue at $\bar{\eta} = \eta_0 + i\Delta$. Thus, $z(t) = \alpha(\eta_0 + i\Delta, t)$.

Please cite this article in press as: P. So, et al., Networks of theta neurons with time-varying excitability: Macroscopic chaos, multistability, and final-state uncertainty, Physica D (2013), http://dx.doi.org/10.1016/j.physd.2013.04.009

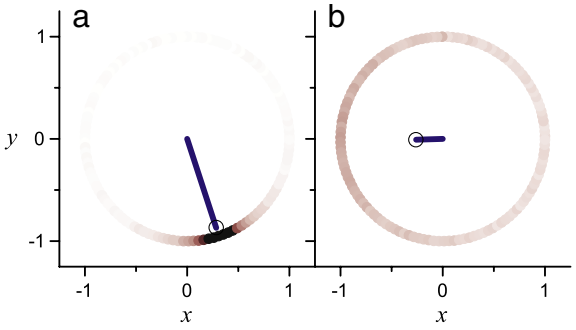

Fig. 3. Macroscopic equilibrium states in the frozen network ($A = 0$). Open circles and blue lines show the attracting equilibria for the macroscopic mean field variable z, obtained using the reduced system, Eq. (18). The red dots show snapshots of the distribution of phases for a finite discrete network of 10,000 oscillators, with darker regions denoting higher density. (a) The partially synchronous rest state (PSR) with $\eta_0 = -0.2$, $k = -0.8$. (b) The partially synchronous spiking state (PSS) with $\eta_0 = 0.2$, $k = 2.0$. $\Delta = 0.1$ in both cases. (For interpretation of the references to colour in this figure legend, the reader is referred to the web version of this article.)

Finally, by substituting f (Eq. (10)) and h (Eq. (11)) into Eqs. (16) and (17) and evaluating at the residue, we obtain

$$\dot{z} = -i\frac{(z-1)^2}{2} + \frac{(z+1)^2}{2}\left[-\Delta + i\eta_0(t) + ikH(z,n)\right], \qquad (18)$$

where the excitability function $\eta_0(t) = \eta_0 + A\sin(2\pi t/\tau)$ varies about the fixed median value η_0 in time and the synaptic function $H(z,n)$ is given by Eqs. (12)–(14). The asymptotic dynamics of Eq. (18) coincides with that of the infinite discrete theta neuron network in Eqs. (2) and (3) [16].

2.2. Macroscopic states of the frozen system

Luke et al. [20] studied the macroscopic dynamics of a "frozen" version of our network, in which the excitability parameters η_j are *fixed* (i.e., $A = 0$ in Eq. (4)). They found three fundamental macroscopic states for this case: a partially synchronous rest state (PSR), a partially synchronous spiking state (PSS), and a collective periodic wave state (CPW). Transitions between these states were examined as the parameters η_0, k, and Δ were varied. Luke et al. [20] also found that the qualitative features of their result do not depend strongly on the choice of the sharpness parameter n. Thus, we have fixed $n = 2$ for all of our numerical examples below.

In the PSR state, the macroscopic mean field z approaches a stable equilibrium (a node) asymptotically [21]. This state is predominantly observed when the distribution of excitability parameters is such that most neurons are in the resting regime ($\eta_0 + \Delta < 0$), and the neurons are coupled through inhibitory synapses ($k < 0$). This macroscopic state calculated using the reduced system, Eq. (18), is marked with an open circle in Fig. 3(a). In a large but finite discrete realization of such a network, most neurons remain quiescent, but those neurons with sufficiently large excitability parameter $\bar{\eta}_j > 0$ spike regularly. A depiction of the microscopic distribution of phases for a finite network ($N = 10{,}000$) at the same parameters is also shown in Fig. 3(a) with red dots, where the shade of red denotes the density of oscillators.

The macroscopic mean field attractor for the PSS state is also a stable equilibrium (a focus). This state typically occurs when most neurons inherently spike ($\eta_0 - \Delta > 0$), and the neurons are coupled through excitatory synapses ($k > 0$). In a finite realization, the majority of neurons spike regularly, but the collective circulation is organized such that the mean field remains fixed. This state is illustrated in Fig. 3(b).

The macroscopic and microscopic behavior exhibited by the PSS and the PSR states described above are analogous to the (somewhat confusingly named) asynchronous state previously studied in [22].

An interesting case occurs when most neurons inherently spike ($\eta_0 - \Delta > 0$), but are coupled though inhibitory synapses ($k < 0$). In this case, there is dynamic competition between the neurons' inherent activity and their inhibitory interaction. In these circumstances, the CPW state can occur: the network exhibits partial coherence that waxes and wanes periodically in time [23] such that the mean field is attracted to a limit cycle. An example of the macroscopic limit cycle is shown in Fig. 4(a), and panels b and c show snapshots of the distribution of phases for the corresponding microstates at different times. One can clearly see the network coherence change as the macroscopic mean field goes around the limit cycle periodically.

Based on a comprehensive bifurcation analysis, Luke et al. [20] conclude that no other macroscopic states beyond the three identified above (PSR, PSS, and CPW) are possible in the frozen network. However, more complicated macroscopic behavior is possible if the neuronal excitability parameters vary in time. In the following, we use the mean field equation derived in the previous section (Eq. (18)) to demonstrate the emergence of macroscopic aperiodicity and multistability in our time-dependent network.

3. Results

3.1. Emergence of macroscopic quasiperiodicity and chaos

Our initial results parallel a similar study [1] in which periodic modulation was introduced into the coupling parameter in a Kuramoto system with a bimodal natural frequency distribution. If the amplitude A of the modulation is small, then in both cases the equilibria of the frozen system (which in our theta neuron network are the PSR and PSS states) become periodic orbits in the time-dependent system. For moderately slow driving, these orbits (which we call librations) have the same period τ as the drive $\eta(t)$. In essence, the system simply follows along as the periodic drive moves the previously frozen equilibrium back and forth.

Similarly, limit cycles of the frozen system, which occur for our network's CPW state, typically become quasiperiodic attractors on a torus in the time-dependent system (again, for small A). This is shown in Fig. 5(a), in which a plot of the quasiperiodic state calculated using Eq. (18) is shown. For comparison, Fig. 5(b) shows the mean field behavior of a large discrete network realization with 10,000 theta neurons, after a sufficiently long transient has been discarded. One can see that the prediction from the reduced mean field equation is quite good. A snapshot showing the microstate at a particular time is shown in Fig. 5(c).

As the amplitude A of the periodic modulation is increased, frequency locking between the macroscopic mean field and the periodic drive $\eta(t)$ is observed. Higher-order periodic orbits emerge from quasiperiodic behavior in a manner similar to that seen in the periodically-driven circle map [24]. However, in our case, frequency locking comes about from the interplay between the periodic drive and the collective rhythm that arises in the network. This can be seen in the bifurcation diagram of Fig. 6. To create this figure, many values of the amplitude A (on the horizontal axis) were selected. For each such value, several asymptotic trajectories of the macroscopic mean field z were obtained using Eq. (18). These trajectories were then stroboscopically sampled at period τ, and the real part of the resulting data was plotted. Since quasiperiodic trajectories are space-filling, this process produced the dark bands visible on the left of the figure. Among these bands, two large windows near $A = 0.38$ and 0.9 can be seen in which the data falls on a discrete number of lines, thus indicating periodic orbits. The smaller window is magnified in the inset. There are an infinite number of such periodic windows within the quasiperiodic bands, but most are too thin to be observed at this magnification.

Please cite this article in press as: P. So, et al., Networks of theta neurons with time-varying excitability: Macroscopic chaos, multistability, and final-state uncertainty, Physica D (2013), http://dx.doi.org/10.1016/j.physd.2013.04.009

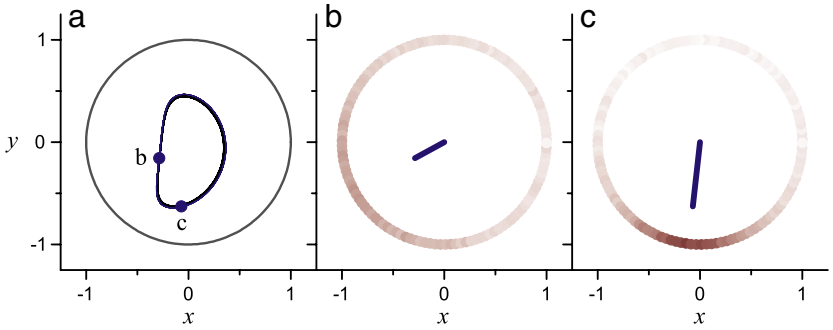

Fig. 4. The collective periodic wave (CPW) state in the frozen network. (a) The attracting limit cycle for the macroscopic mean field z with $\eta_0 = 10.75$, $k = -9.0$, and $\Delta = 0.5$. On this scale, there is no visible difference between the limit cycle obtained with Eq. (18) and that calculated with a discrete network of 10,000 neurons. The labeled dots on the limit cycle correspond to the snapshots shown in (b) and (c), taken at different times. The red dots show snapshots of the distribution of phases in the discrete network at the same parameters, with darker regions denoting higher density. The blue lines indicate the instantaneous macroscopic mean field variable z. (For interpretation of the references to colour in this figure legend, the reader is referred to the web version of this article.)

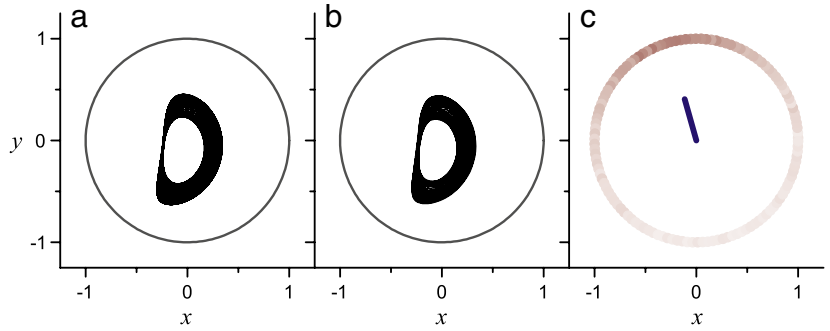

Fig. 5. The macroscopic quasiperiodic state. (a) The predicted attractor, obtained using Eq. (18) with $\eta_0 = 10.75$, $k = -9$, $\Delta = 0.5$, $A = 0.7625$, and $\tau = 1$. (b) The asymptotic trajectory of the macroscopic mean field, obtained using a network of 10,000 theta neurons and the same parameters. (c) A snapshot showing the instantaneous macroscopic mean field (blue line) of the discrete network at a particular time. In addition, the red dots show the corresponding distribution of phases in the discrete network, with darker regions denoting higher density. (For interpretation of the references to colour in this figure legend, the reader is referred to the web version of this article.)

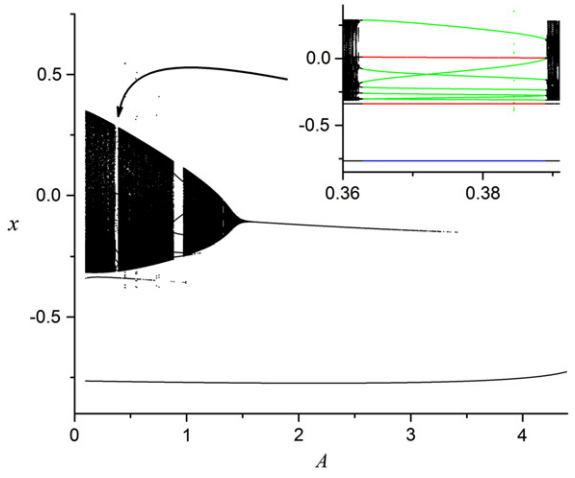

Fig. 6. Bifurcation diagram showing the asymptotic behavior of the macroscopic mean field, obtained using Eq. (18), versus the amplitude A of the excitability modulation (defined in Eq. (4)). The macroscopic mean field z was sampled stroboscopically with period τ before $x = Re(z)$ was plotted, and many initial conditions were used for each value of A in order to identify coexisting attractors. Other parameters were $\eta_0 = 10.75$, $k = -9$, $\Delta = 0.5$, and $\tau = 1$. The structure with dark bands on the left reflects quasiperiodic behavior. Periodic orbits appear as sets of lines. The inset is a magnification showing the thin periodic window near $A = 0.38$. The three coexisting periodic orbits within this window are color coded according to the color scheme used in Fig. 11. (For interpretation of the references to colour in this figure legend, the reader is referred to the web version of this article.)

The trajectories that were used in the construction of Fig. 6 were calculated using many different initial conditions in order to reveal the presence of coexisting attractors. (Note that we did not necessarily find *all* the attractors.) For example, two periodic orbits that coexist with the quasiperiodic bands are clearly visible. A prominent one is near $x = -0.75$. This corresponds to a small libration and has period τ; hence it appears in the figure as a single line. Another coexisting periodic orbit is visible near $x = -0.33$. This orbit is plotted in red in the inset, and appears as two lines, revealing that it is a period-2τ orbit. (The period of a periodic orbit is defined by the smallest $T > 0$ such that $z(t) = z(t+T)$; we call an orbit period-$m\tau$ if $T = m\tau$.)

Restricting attention to the periodic window that is magnified in the inset, we see that three periodic orbits coexist here: the period-τ (blue) and period-2τ (red) orbit mentioned above, and a period-7τ orbit that is plotted in green. (Fig. 11 shows a state-space representation of the three coexisting orbits at $A = 0.38$ using the same color scheme.)

Sequences of bifurcations near the period-2τ orbit appear near $A = 0.5$. These, along with other bifurcation cascades that are difficult to resolve, lead to the creation of a chaotic saddle which eventually becomes attracting. This can be seen in Fig. 7, which is a continuation of Fig. 6 to higher values of the amplitude A. (The lower panel shows the two largest Lyapunov exponents, confirming the presence of chaos.) The first attracting chaotic band appears at a crisis when the chaotic saddle and an unstable period-τ orbit collide near $A = 4.525$. Note that there is a small region in which the libration (a stable period-τ orbit) coexists with the stable chaotic band. For higher values of A, multiple chaotic bands delineated by period doubling cascades on the right and crises on the left can be seen. Also visible near $A = 5.65$ is a smaller cascade from a period-6τ orbit that coexists with the main branch. Many such regions of multistability are present, and their dynamical implications for the full network will be examined in more detail in the next section.

Please cite this article in press as: P. So, et al., Networks of theta neurons with time-varying excitability: Macroscopic chaos, multistability, and final-state uncertainty, Physica D (2013), http://dx.doi.org/10.1016/j.physd.2013.04.009

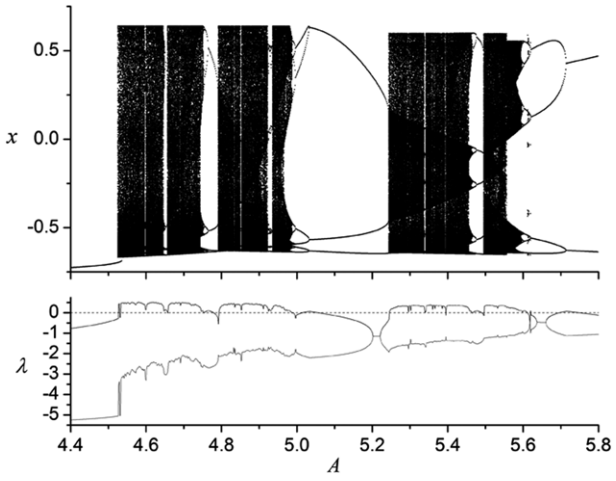

Fig. 7. (Top) A continuation of Fig. 6 to higher values of A, showing the emergence of macroscopic chaos. (Bottom) The corresponding two largest Lyapunov exponents of the most dominant attractors seen in the top panel.

A phase portrait of the chaotic attractor for $A = 4.8$ calculated using the reduced system, Eq. (18), is shown in Fig. 8(a), and the corresponding mean field behavior for the finite network ($N = 10{,}000$) is shown in panel b. Panel c shows a snapshot of the microstate. The trajectory from the reduced mean field equation traces out an attractor which matches very well with the one calculated directly from the full discrete network. We emphasize that chaotic attractors for the macroscopic mean field were only observed in parameter space regions in which there is competition between the intrinsic spiking behavior of the neurons ($\eta_0 > 0$) and inhibitory synaptic coupling ($k < 0$).

A similar sequence of bifurcations into and out of quasiperiodicity and chaos can be seen if one varies the period τ of the time-varying network excitability $\eta(t)$. This is shown in Fig. 9, which was obtained with $A = 4.8$ and the remaining parameters fixed as above. The three panels show several of the network's attractors for fast, moderate, and slow modulation of $\eta_0(t)$ (i.e., increasing periods τ). Panels (a) and (b) were constructed in the same manner as Figs. 6 and 7. That is, the asymptotic values of $x = Re(z)$ were obtained using Eq. (18) with many different initial conditions, and the resulting attractors were sampled stroboscopically at period τ.

For fast modulation (Fig. 9(a)), the macroscopic mean field exhibits quasiperiodic behavior similar to that described above with small amplitude modulation (see Fig. 6). For moderate modulation (Fig. 9(b)), a more dynamically rich regime is found. As before, there is a region (τ approximately in [0.4, 0.9]) in which many bifurcation cascades are found (some of which are difficult to resolve), after which attracting chaotic bands occur that are again bracketed by crises and period-doubling cascades.

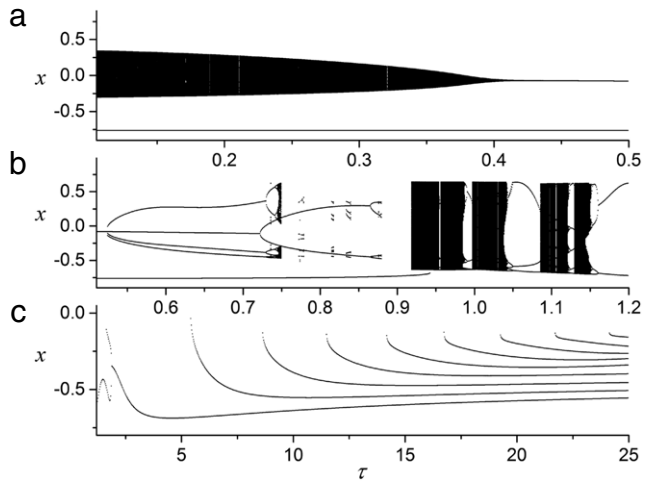

Fig. 9. Bifurcation diagrams showing the asymptotic behavior of the macroscopic mean field, obtained using Eq. (18), versus the period τ of the excitability modulation (defined in Eq. (4)). Many initial conditions were used in order to identify coexisting attractors. The panels show ranges of (a) fast, (b) moderate, and (c) slow modulation. In panels (a) and (b), the macroscopic mean field z was sampled stroboscopically with period τ before $x = Re(z)$ was plotted. In panel (c), z was sampled using a Poincaré surface of section at $y = Im(z) = -0.3$ before $x = Re(z)$ was plotted. This was done in order to show that the winding number of the attractor increases in a sequence of period-adding bifurcations. Other system parameters for all three graphs were $\eta_0 = 10.75$, $k = -9$, $\Delta = 0.5$, and $A = 4.8$.

Finally, for very slow modulation ($\tau > 1.2$), no more chaos is found. However, as τ is increased further, a sequence of period-adding bifurcations [25] occurs, as shown in Fig. 9(c). In this region, a period-τ orbit increases its winding number by one at each such bifurcation. To reflect this, the bifurcation diagram in this panel was obtained using a Poincaré surface of section at $y = -0.3$, instead of the stroboscopic map used in previous diagrams. We denote a period-$m\tau$ orbit with winding number w as period-$m\tau_w$. Fig. 10 shows the phase portrait of the period-τ_9 orbit at $\tau = 25$. The bifurcation diagram (Fig. 9(c)) shows that this period-τ_9 orbit emerges from a period-τ_1 orbit by acquiring an additional twist each time τ increases through the following sequence of bifurcation points: $\tau = 5.5$, 8.7, 11.5, 14.2, 16.8, 19.3, 21.7, and 24.2.

To conclude this section, we note that naively, one might typically expect two default behaviors to be present in the mean field dynamics for a large heterogeneous network of neuronal oscillators. At one extreme, with little or no coupling, one might expect the neurons to behave incoherently, so that the macroscopic mean field in some sense "averages out". At the other extreme, one might expect that sufficiently strong coupling would lead to network synchrony. We have demonstrated in this section that the actual situation, even in the frozen case, is more nuanced.

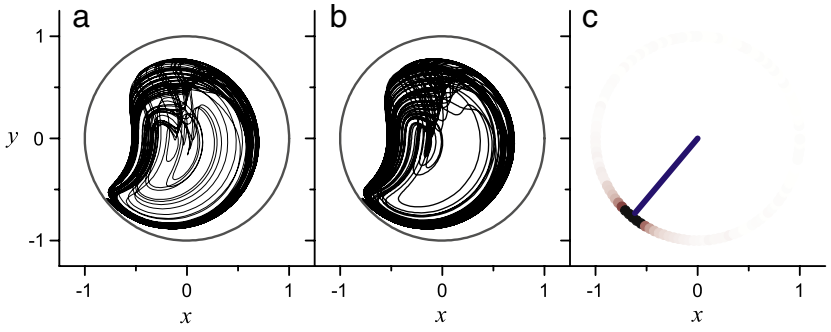

Fig. 8. (a) A predicted chaotic attractor, obtained using the reduced mean field equation (Eq. (18)) with $\eta_0 = 10.75$, $k = -9$, $\Delta = 0.5$, $A = 4.8$, and $\tau = 1$. (b) The asymptotic trajectory of the macroscopic mean field, obtained using a discrete network of 10,000 neurons at the same parameters. (c) A snapshot showing the microstate at a particular time. The blue line indicates the instantaneous macroscopic mean field variable z, and the red dots show the distribution of phases, with darker regions denoting higher density. (For interpretation of the references to colour in this figure legend, the reader is referred to the web version of this article.)

Please cite this article in press as: P. So, et al., Networks of theta neurons with time-varying excitability: Macroscopic chaos, multistability, and final-state uncertainty, Physica D (2013), http://dx.doi.org/10.1016/j.physd.2013.04.009

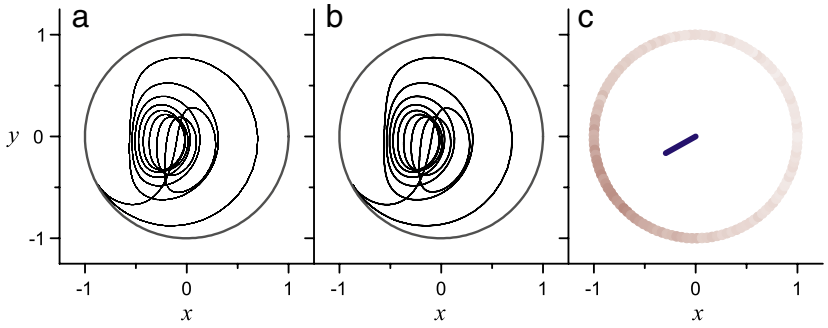

Fig. 10. The period-τ_9 orbit with winding number 9 created by the sequence of period-adding bifurcations shown in Fig. 9(c). (a) The predicted orbit obtained using the reduced mean field equation (Eq. (18)) with $\eta_0 = 10.75$, $k = -9$, $\Delta = 0.5$, $A = 4.8$, and $\tau = 25$. (b) The asymptotic trajectory of the macroscopic mean field, obtained using a discrete network of 10,000 neurons at the same parameters. (c) A snapshot showing the microstate at a particular time. The blue line indicates the instantaneous macroscopic mean field variable z, and the red dots show the distribution of phases, with darker regions denoting higher density. (For interpretation of the references to colour in this figure legend, the reader is referred to the web version of this article.)

Furthermore, a richer set of dynamical states are possible when one introduces temporal variation into the neuronal excitability parameters. Quasiperiodic and even chaotic behavior are possible in the collective behavior of such networks.

3.2. Multistability and final state uncertainty

The bifurcation diagrams presented in the previous section demonstrate that multistability is easy to find in the macroscopic dynamics of our network. There are parameter ranges in which periodic orbits coexist with different periodic orbits, quasiperiodic orbits coexist with periodic orbits, and chaos coexists with periodic orbits. We used the macroscopic mean field equation (Eq. (18)), which we derived using the OA reduction method (Section 2.1), to identify these attractors. As described above, the asymptotic behavior of Eq. (18) coincides with the asymptotic behavior of the large discrete network defined by Eqs. (2)–(5).

It is important to note, however, that the transient behavior of Eq. (18) does not correspond to the transient behavior of the discrete network. Consequently, the reduced equation cannot be used to calculate basins of attraction for the discrete network. In general, the transient behavior of the macroscopic mean field z, and the identity of which attractor is ultimately reached, depends on the network's *microscopic* initial conditions [19]. We show here that for our discrete network (Eqs. (2)–(5)), the boundary between different basins of attraction in multistable regions can be fractal, and consequently, the macroscopic mean field z exhibits final state sensitivity [26].

We focus on the following parameters, for which the network possesses three coexisting attractors: $\eta_0 = 10.75$, $k = -9$, $\Delta = 0.5, A = 0.38$, and $\tau = 1$. These attractors are shown in Fig. 11. The innermost attractor, in green, is a period-7τ orbit. Encircling this is a large period-2τ orbit shown in red. The third attractor, in blue and near ($x = -0.75$, $y = -0.62$), is the small period-τ libration mentioned above. All three of these are visible in the inset of the stroboscopic bifurcation diagram of Fig. 6.

Initial conditions for the discrete network can be specified by a complete set of initial phase angles $\{\theta_j(t=0)\}_{j=1}^{N}$. But rather than having to specify N phases individually, it has been shown that for systems such as ours, it is sufficient to specify the initial values of just three quantities, known as the Watanabe–Strogatz (WS) variables [15]. See Appendix B for details. On the OA manifold, the first two WS variables are related to the real and imaginary parts of the macroscopic mean field $z = x + iy$. The remaining WS variable, Φ, is an additional degree of freedom that essentially describes the spread of the oscillator phases with respect to the mean phase of the population. Since our network also includes the time-dependent excitability modulation defined in Eq. (4),

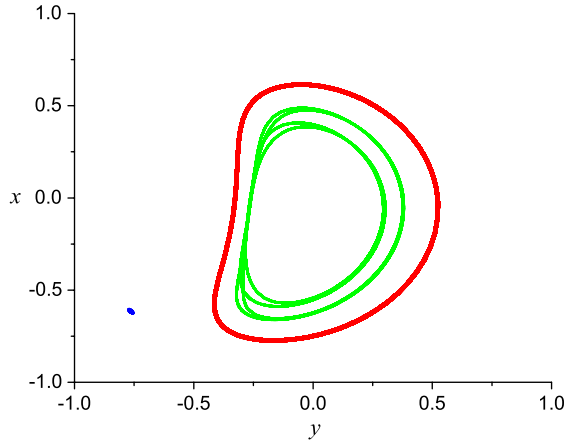

Fig. 11. Three coexisting periodic orbits predicted from the reduced mean field equation, Eq. (18), with $\eta_0 = 10.75$, $k = -9$, $\Delta = 0.5$, $A = 0.38$, and $\tau = 1$. The period m of an orbit is determined by the condition $z(t) = z(t + m\tau)$. The inner orbit (green) is a period-7τ orbit. The large outer orbit (red) has period 2τ. The third attractor is the small period-τ libration near the lower left corner (blue). In the x–y macroscopic state space, the period-2τ orbit appears as a single loop since it takes the trajectory 2τ time units to come back onto itself. Similarly, the period-7τ orbit takes 7τ time units to complete four cycles around the origin. (For interpretation of the references to colour in this figure legend, the reader is referred to the web version of this article.)

the initial phase shift δ_0 must also be specified. Thus, we have a four-dimensional space $(x_0, y_0, \delta_0, \Phi_0)$ of initial conditions for our discrete N-neuron network.

In order to visualize this space, we take a two-dimensional slice at $x_0 = 0.45$ and $y_0 = -0.3$, and select a point on the resulting δ_0–Φ_0 plane. Then, we integrate the discrete network with 10,000 neurons using Eqs. (2)–(5). Transients are discarded, and the pixel at the selected point (δ_0, Φ_0) is colored according to the color scheme of Fig. 11 to label which attractor is attained. If this cannot be determined in a reasonable time, or if the trajectory settles on an attractor different from the three identified above, the point is plotted without color. This process is then repeated to fill out an interesting region of the δ_0–Φ_0 plane.

The result is shown in Fig. 12(a) and (b). One can clearly identify large solid-color basins for each attractor, and the boundaries appear to be fractal. (Indeterminate points only occur in the lower part of panel a.) Fig. 12(b) is a magnification of the area marked by the small rectangle in Fig. 12(a). The fractal structure of the basin boundary [26] can be seen, including the possible intermingling of the three basins, despite the fuzziness due to the finite size of the network [27]. We conjecture that the boundary becomes a mathematically true fractal (which may have the Wada property [28]) as $N \to \infty$.

Please cite this article in press as: P. So, et al., Networks of theta neurons with time-varying excitability: Macroscopic chaos, multistability, and final-state uncertainty, Physica D (2013), http://dx.doi.org/10.1016/j.physd.2013.04.009

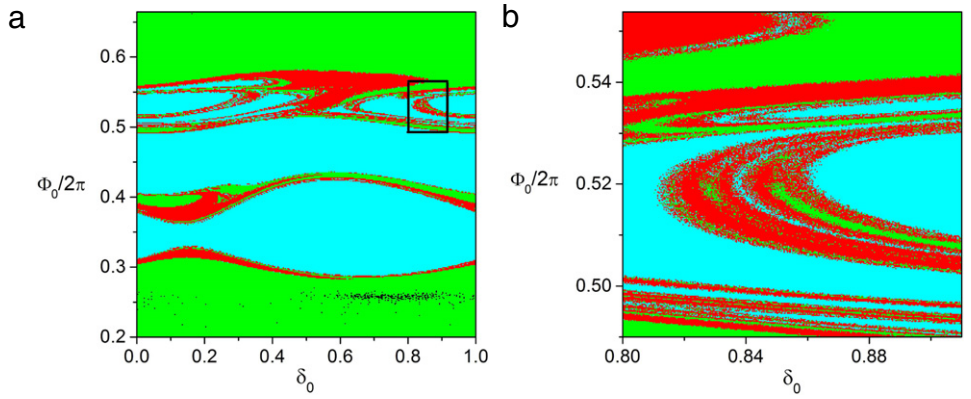

Fig. 12. Basins of attraction for the attractors shown in Fig. 11, obtained using a discrete network of 10,000 neurons. Panel (b) is a magnification of the region marked by the black rectangle in panel (a). Initial conditions for the discrete network consist of a point (δ_0, Φ) on this graph, with $x_0 = 0.45$ and $y_0 = -0.3$.

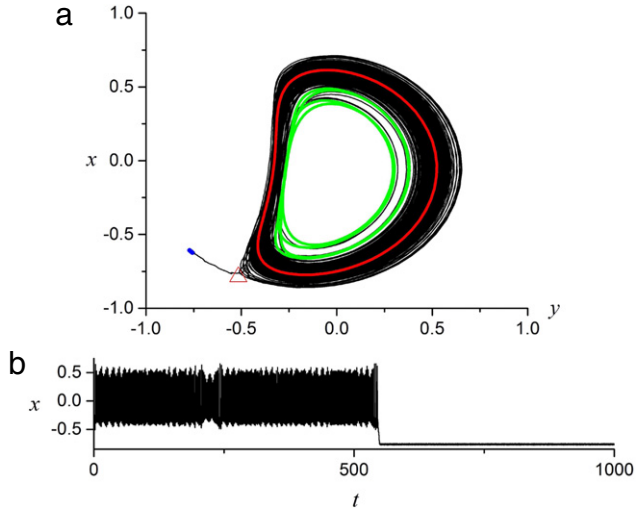

Fig. 13. (a) A trajectory (black) of the macroscopic mean field obtained using a small network of 2000 neurons illustrating fluctuation-induced escape. Parameters are as in Fig. 11. The red limit cycle is the predicted period-2τ attractor obtained from the reduced mean field equation (Eq. (18)). The black trajectory follows the predicted trajectory for approximately 500 time units before it escapes to the small period-τ libration in the lower left corner. The innermost period-7τ orbit is also shown in green in this figure. (b) A plot of the real part x of the macroscopic mean field versus time. (For interpretation of the references to colour in this figure legend, the reader is referred to the web version of this article.)

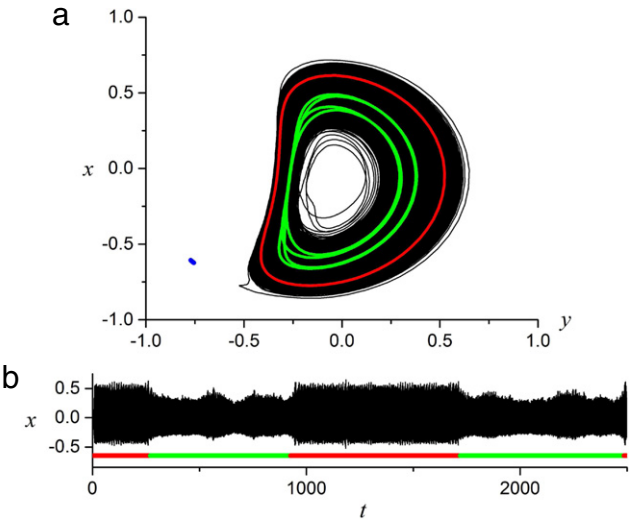

Fig. 14. (a) A trajectory (black) of the macroscopic mean field obtained using a small network of 2000 neurons illustrating fluctuation-induced intermittency. Parameters are as in Fig. 11. The trajectory switches between the inner period-7τ attractor (green) and the outer period-2τ attractor (red) due to finite network-size fluctuations. (b) A plot of the real part x of the macroscopic mean field versus time showing the intermittent switching behavior. The time intervals in which the black trajectory visits each attractor are labeled by the colored bars on the bottom of the graph. (For interpretation of the references to colour in this figure legend, the reader is referred to the web version of this article.)

We conclude this section by emphasizing that the fractal nature of the basin boundaries is a feature of the discrete network. The reduced mean field equation can be used to identify the asymptotic macroscopic attractors of the network, but the transient behavior and basin structure of the network is determined by the discrete network dynamics only upon full specification of the initial microscopic state.

3.3. Macroscopic switching and intermittency

The fuzziness of Fig. 12(b) suggests that fluctuations due to the finite nature of a discrete network play an important role in determining the asymptotic behavior of the macroscopic mean field z. Since such fluctuations scale as $1/\sqrt{N}$, we expect that smaller networks would be more affected.

For multistable systems, one consequence is that asymptotic stability is compromised. As the size of a discrete network decreases, the probability of a fluctuation "kicking" a trajectory from near one attractor into the basin of a different attractor increases. To illustrate this, we used a small network with only 2000 neurons and with the same parameters as in Fig. 11. We chose an initial condition near the boundary between the red and blue basins of Fig. 12, specifically, $x_0 = 0.45$, $y_0 = -0.30$, $\delta_0 = 0.165$, and $\Phi_0/2\pi = 0.32$. Fig. 13 shows the evolution of the real part of the macroscopic mean field from this initial condition. Initially, the trajectory is attracted to the large orbit shown in red. The noisiness of this trajectory is likely enhanced due to the presence of several nearby unstable periodic orbits. After spending a long time there, a fluctuation by chance kicks the trajectory into the basin of the period-τ libration when it happens to visit a saddle-like structure [29] labeled by the open red triangle. The trajectory then escapes to the libration, which is smaller. This attractor is more isolated with fewer unstable periodic orbits nearby as compared to the central region of state space, and hence the subsequent trajectory is less noisy.

If instead we choose the initial condition to be near the boundary between the red and the green regions of Fig. 12 at $x_0 = 0.45$, $y_0 = -0.30$, $\delta_0 = 0.50$, $\Phi_0/2\pi = 0.565$, we observe intermittent switching between the two large periodic orbits. This is shown in Fig. 14. This intermittent behavior introduces a low-frequency alternation in the temporal signal of the macroscopic

Please cite this article in press as: P. So, et al., Networks of theta neurons with time-varying excitability: Macroscopic chaos, multistability, and final-state uncertainty, Physica D (2013), http://dx.doi.org/10.1016/j.physd.2013.04.009

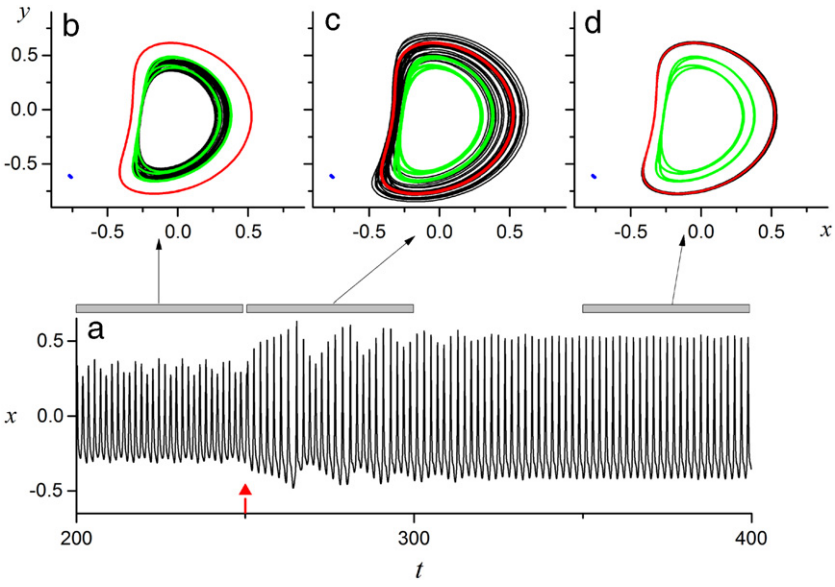

Fig. 15. A trajectory (black) of the macroscopic mean field obtained using a network of 10,000 neurons illustrating a perturbation-induced switch. Parameters are as in Fig. 11. The lower panel (a) shows a plot of the real part x of the macroscopic mean field versus time. A perturbation is applied to the phase of the excitability modulation at $t = 250$ time units (red arrow), causing the switch. The upper panels show the state-space trajectories of the data in the intervals marked with the gray bars. The attractors of Fig. 11 are superimposed for reference. (For interpretation of the references to colour in this figure legend, the reader is referred to the web version of this article.)

dynamics that is not intrinsic to the natural time scales of the individual neurons. Similar emergent low-frequency behavior was recently reported in networks of inhibitory hippocampal neurons [30].

An interesting difference between this macroscopic intermittent behavior and the previously-described escape behavior is that in the intermittent situation, both macroscopic "attractors" become non-attracting in the smaller network, while in the escape example, the small libration remains locally attracting even for the small network.

Finally, we show that it is possible to deliberately effect a switch between coexisting attractors of the macroscopic mean field in larger networks by applying a small, short perturbation. This is shown using the larger network of 10,000 neurons, with the same parameters as before, in Fig. 15. A trajectory that is initially near the period-7τ attractor is shown. At time $t = 250$ (arbitrary units), the phase of the sinusoidal modulation in η is shifted abruptly by 0.2π. This causes the macroscopic mean field trajectory to shift, after an oscillating transient, to the larger period-2τ attractor. Subsequently, the trajectory remains there indefinitely.

4. Conclusion

We constructed a large heterogeneous network of coupled theta neurons that interact globally via pulse-like synapses and whose excitability parameter varies sinusoidally in time. This idealization allowed us to apply recently-developed analytical techniques to identify the asymptotic behavior of the macroscopic mean field dynamics of the network. We showed that macroscopic chaos, quasiperiodicity, multistability, and final-state uncertainty are all exhibited by this non-autonomous network.

The assumption of global coupling is necessary for the derivation of Eq. (18). Of course, this assumption does not apply to many real-world networks of interest. Nevertheless, we believe that the insights gleaned from our approach are useful in that they identify dynamical states and behavior that one might begin to investigate in imperfectly-coupled networks. For example, we have found that the reduced system gives a reasonably accurate description of the full discrete network's behavior even if 10%–15% of the links are randomly removed (this claim will be made more precise in [31]). Similarly, the assumption of constant synaptic strength k is at best a rough approximation when describing real biological networks. Our reduction method, however, does not preclude the analysis of a network in which the synaptic strengths are given by a distribution of values. We are currently investigating such systems.

Our work demonstrates the utility and the limitations of the reduced mean-field equation, Eq. (18). This can be used to identify attractors of the macroscopic mean field z, and to identify parameter space regions in which attractors coexist. However, understanding the transient behavior of the full discrete network, including the structure of attractor basins, requires detailed specification of the full network microstates. Furthermore, fluctuations due to the finite number of neurons in a real or simulated network must be considered. For smaller networks, these fluctuations play an important role in the mean field dynamics. Finally, we demonstrated that simple control of the macroscopic behavior of networks with a small global perturbation is possible. A more detailed and expanded study of the former will be presented in another publication [31].

Appendix A. Derivation of the rescaled synaptic function $H(z, n)$

Applying the binomial theorem twice, the sharpness factor $(1-\cos\theta)^n$ in our synaptic function can be written as a double sum,

$$(1-\cos\theta)^n = \sum_{j=0}^{n}\sum_{m=0}^{j} Q_{jm} e^{i(j-2m)\theta}, \tag{A.1}$$

where

$$Q_{jm} = \frac{(-1)^j n!}{2^j m!(n-j)!(j-m)!}. \tag{A.2}$$

In the continuum limit ($N \to \infty$), one can define a set of Daido moments z_q [32] with $q \in \mathbb{Z}$ to characterize the macroscopic mean field of the network,

$$z_q(t) = \int_{-\infty}^{\infty}\int_{0}^{2\pi} \rho(\theta, \bar{\eta}, t) e^{iq\theta} d\theta d\bar{\eta}, \tag{A.3}$$

Please cite this article in press as: P. So, et al., Networks of theta neurons with time-varying excitability: Macroscopic chaos, multistability, and final-state uncertainty, Physica D (2013), http://dx.doi.org/10.1016/j.physd.2013.04.009

and the rescaled synaptic current can then be written in terms of these Daido moments,

$$H = \frac{I_{syn}}{k} = a_n \int_{-\infty}^{\infty}\int_0^{2\pi} \rho(\theta,\bar{\eta},t)(1-\cos\theta)^n$$
$$= a_n \sum_{l=0}^{n}\sum_{m=0}^{j} Q_{jm}\left[\int_{-\infty}^{\infty}\int_0^{2\pi} \rho(\theta,\bar{\eta},t)e^{i(j-2m)\theta}\right]$$
$$= a_n \sum_{j=0}^{n}\sum_{m=0}^{j} Q_{jm} z_{j-2m}. \tag{A.4}$$

Now, the double sum on z_{l-2m} can be expanded and regrouped into a single sum on $(z_q + z_{-q})$ with $q = 0, \ldots, n$,

$$H(z_q, n) = a_n\left(C_0 + \sum_{q=1}^{n} C_q\left[z_q + z_{-q}\right]\right), \tag{A.5}$$

where

$$C_q = \sum_{j,m=0}^{n} \delta_{j-2m,q} Q_{jm},$$

and $z_0 = 1$ since ρ is assumed to be normalized. Note that $H(z_q, n)$ in the above equation depends on all statistical moments z_q of the macroscopic mean field with all q from $-n$ to n. In the following, we will show that the qth statistical moment simply equals the qth power of the first moment, i.e., $z_q(t) = z^q(t)$ $[q \geq 0]$ and $z_q(t) = (z^*)^{|q|}$ $[q < 0]$, if the network excitability distribution function $g(\bar{\eta})$ is given by the Lorentzian distribution. In this special case, $H(z, n)$ can be further reduced to a function depending on the first moment $z \equiv z_1$ of the macroscopic mean field only.

For a heterogeneous network such as ours, the general Daido moment z_q can be explicitly evaluated by directly substituting $\rho(\theta, \bar{\eta}, t)$, as given by the OA ansatz in Eq. (15), into its definition,

$$z_q(t) = \int_{-\infty}^{\infty}\int_0^{2\pi} \frac{g(\bar{\eta})}{2\pi}\left\{e^{iq\theta} + \sum_{j=1}^{\infty}\left[\alpha^*(\bar{\eta},t)^j e^{i(q+j)\theta} + \alpha(\bar{\eta},t)^j e^{i(q-j)\theta}\right]\right\} d\theta d\bar{\eta}.$$

Exchanging the order of the infinite sum with the two definite integrals, all terms in the sum are now proportional to the delta function,

$$\delta(q \pm j) = \frac{1}{2\pi}\int_0^{2\pi} e^{i(q\pm j)}d\theta,$$

with $j \in \mathbb{N}$. Thus, the infinite sum collapses to a single term, and we have

$$z_q(t) = \begin{cases} \displaystyle\int_{-\infty}^{\infty} g(\bar{\eta})\alpha^*(\bar{\eta},t)^{|q|}d\bar{\eta}, & q < 0 \\ 1, & q = 0 \\ \displaystyle\int_{-\infty}^{\infty} g(\bar{\eta})\alpha(\bar{\eta},t)^q d\bar{\eta}, & q > 0. \end{cases} \tag{A.6}$$

Similar to the discussion in the main text following Eq. (17), the $\bar{\eta}$-integral can be evaluated in closed form if $g(\bar{\eta})$ is given by the Lorentzian distribution function Eq. (5). Specifically, we can analytically continue $g(\bar{\eta})$ into the upper complex $\bar{\eta}$ plane and the normalized Lorentzian distribution can be rewritten as,

$$g(\bar{\eta}) = \frac{\Delta}{\pi}\frac{1}{(\bar{\eta} - (\eta_0 + i\Delta))(\bar{\eta} - (\eta_0 - i\Delta))}.$$

One can clearly see that $g(\bar{\eta})$ has two simple poles $\bar{\eta} = \eta_0 \pm i\Delta$ with one in the upper half of the complex $\bar{\eta}$ plane, and the other in the lower half. Then, by choosing an infinite semi-circle contour in the upper $\bar{\eta}$ plane to close our integral, z_q can immediately be evaluated at its residue $\bar{\eta} = \eta_0 + i\Delta$,

$$z_q(t) = \begin{cases} \alpha^*(\eta_0 + i\Delta, t)^{|q|}, & q < 0 \\ 1, & q = 0 \\ \alpha(\eta_0 + i\Delta, t)^q, & q > 0. \end{cases} \tag{A.7}$$

Finally, by defining $z(t) \equiv z_1(t) = \alpha(\eta_0 + i\Delta)$ to be the first Daido moment, Eq. (A.7) makes it evident that the remaining Daido moments $z_q(t)$ can be expressed as the qth powers of the first moment $z(t)$, i.e., $z_q(t) = z^q(t)$ $[q \geq 0]$ and $z_q(t) = (z^*)^{|q|}$ $[q < 0]$. Substituting this result into Eq. (A.5), we then have our desired expression for $H(z, n)$, Eq. (12).

Appendix B. The Watanabe–Strogatz variables

Here we provide additional details regarding the specification of initial conditions for the discrete network. In Ref. [14], Marvel et al. show that the set of phase variables $\{\theta_j(t)\}_{j=1}^N$ of any network given by the sinusoidally coupled form of Eq. (9), such as our theta neuron network, possesses an extraordinary degree of symmetry given by the Möbius transformation

$$\tan\left[\frac{\theta_j(t) - \Psi(t)}{2}\right] = \frac{1-\sigma(t)}{1+\sigma(t)}\tan\left[\frac{\psi_j - \Phi(t)}{2}\right], \tag{B.1}$$

for $j = 1, \ldots, N$. Here, $\{\psi_j\}_{j=1}^N$ is a set of N constants of motion, and $\sigma(t)$, $\Psi(t)$, and $\Phi(t)$ are known as the Watanabe–Strogatz (WS) variables [15]. (We have written Eq. (B.1) in the form given in Ref. [19]). Remarkably, through the above transformation equation, the N phase variables $\{\theta_j(t)\}_{j=1}^N$ are mapped to the N constants of motion, and the three Watanabe–Strogatz variables carry all the temporal dynamics of the N-dimensional discrete network. This remarkable property is a direct consequence of the sinusoidal form of the globally coupled network [14]. It can be shown that the OA manifold, in which the asymptotic mean field dynamics of our network resides, corresponds to the special case in which the WS constants of motion $\{\psi_j\}_{j=1}^N$ are evenly distributed on the unit circle [18,19,14]. When the network dynamics is restricted to the OA manifold, two of the WS variables are directly related to the macroscopic mean field: $z = re^{i\phi} = \sigma e^{i\Psi}$. The remaining WS variable, Φ, is an additional macroscopic degree of freedom that essentially describes the spread of the oscillator phases with respect to the mean phase of the population.

To construct the full microscopic initial conditions for our discrete network, we specify a desired macroscopic mean field z as well as a value of Φ. Then we use Eq. (B.1), with the constraint that the WS constants of motion be uniformly distributed on $[0, 2\pi]$, to identify a full set of initial phase angles $\{\theta_j\}_{j=1}^N$.

References

[1] P. So, E. Barreto, Chaos 21 (2011) 033127.
[2] A.L. Hodgkin, J. Physiol. 107 (1948) 165–181.
[3] B. Ermentrout, Neural Comput. 8 (1996) 979–1001.
[4] E. Izhikevich, Dynamical Systems in Neuroscience: The Geometry of Excitability and Bursting, MIT Press, Cambridge, MA, 2007.
[5] L.G. Nowak, R. Azouz, M.V. Sanchez-Vives, C.M. Gray, D.A. McCormick, J. Neurophysiol. 89 (2003) 1541–1566.
[6] T. Tateno, A. Harsch, H.P.C. Robinson, J. Neurophysiol. 92 (2004) 2283–2294.
[7] G.B. Ermentrout, N. Kopell, SIAM J. Appl. Math. 46 (1986) 233–253.
[8] G. Buzsaki, Rhythms of the Brain, Oxford University Press, USA, 2006.
[9] E. Barreto, J.R. Cressman Jr., J. Biol. Phys. 37 (2011) 361–373.
[10] J.R. Cressman Jr., G. Ullah, J. Ziburkus, S.J. Schiff, E. Barreto, J. Comput. Neurosci. 26 (2009) 159–170; J. Comput. Neurosci. 30 (2011) 781 (erratum).
[11] J.T. Ariaratnam, S.H. Strogatz, Phys. Rev. Lett. 86 (2001) 4278–4281.
[12] Y. Kuramoto, in: H. Araki (Ed.), International Symposium on Mathematical Problems in Theoretical Physics, in: Lecture Notes in Physics, vol. 39, Springer-Verlag, Berlin, 1975.

Please cite this article in press as: P. So, et al., Networks of theta neurons with time-varying excitability: Macroscopic chaos, multistability, and final-state uncertainty, Physica D (2013), http://dx.doi.org/10.1016/j.physd.2013.04.009

[13] Y. Kuramoto, Chemical Oscillations, Waves and Turbulence, Springer, 1984, pp. 75–76;
J.D. Crawford, J. Stat. Phys. 74 (1994) 1047;
S.H. Strogatz, Physica D 143 (2000) 1;
J.A Acebrón, L.L. Bonilla, C.J. Pérez Vicente, F. Ritort, R. Spigler, Rev. Modern Phys. 77 (2005) 137.
[14] S.A. Marvel, R.E. Mirollo, S.H. Strogatz, Chaos 19 (2009) 043104.
[15] S. Watanabe, S.H. Strogatz, Physica D 74 (1994) 197.
[16] E. Ott, T.M. Antonsen, Chaos 18 (2008) 037113;
E. Ott, T.M. Antonsen, Chaos 19 (2009) 023117.
[17] S.A. Marvel, S.H. Strogatz, Chaos 19 (2009) 013132;
E.A. Martens, E. Barreto, S.H. Strogatz, E. Ott, P. So, T.M. Antonsen, Phys. Rev. E 79 (2009) 026204;
D.M. Abrams, R. Mirollo, S.H. Strogatz, D.A. Wiley, Phys. Rev. Lett. 101 (2008) 084103;
T.M. Antonsen Jr., R.T. Faghih, M. Girvan, E. Ott, J. Platig, Chaos 18 (2008) 037113;
L.F. Lafuerza, P. Colet, R. Toral, Phys. Rev. Lett. 105 (2010) 084101;
W.S. Lee, E. Ott, T.M. Antonsen, Phys. Rev. Lett. 103 (2009) 044101;
C.R. Laing, Chaos 19 (2009) 013113;
C.R. Laing, Physica D 238 (2009) 1569–1588;
L.M. Alonso, J.A. Alliende, G.B. Mindlin, Eur. Phys. J. D 60 (2010) 361;
L.M. Alonso, G.B. Mindlin, Chaos 21 (2011) 023102.
[18] A. Pikovsky, M. Rosenblum, Phys. Rev. Lett. 101 (2008) 264103.
[19] A. Pikovsky, M. Rosenblum, Physica D 240 (2011) 872–881.
[20] T. Luke, E. Barreto, P. So, unpublished.
[21] In the case of a large but finite network, the two macroscopic equilibrium states (PSR and PSS) appear subject to small jitters due to the finite size of the network.
[22] L.F. Abbott, C. van Vreeswijk, Phys. Rev. E 48 (1993) 1483–1490;
D. Hansel, G. Mato, Phys. Rev. Lett. 86 (2001) 4175–4178;
D. Hansel, G. Mato, Neural Comput. 15 (2003) 1–56;
D. Hansel, G. Mato, C. Meunier, Neural Comput. 7 (1995) 307–337.
[23] G.B. Ermentrout, J. Comput. Neurosci. 5 (1998) 191–208;
P.C. Bressloff, Phys. Rev. Lett. 82 (1999) 2979–2982;
R. Osan, J. Rubin, B. Ermentrout, SIAM J. Appl. Math. 62 (2002) 1197–1221.
[24] D. Ruelle, F. Takens, Comm. Math. Phys. 20 (1971) 167–192;
D. Rand, S. Ostlund, J. Sethna, E.D. Siggia, Phys. Rev. Lett. 49 (1982) 132–135;
E. Ott, Chaos in Dynamical Systems, second ed., Cambridge University Press, 1993, pp. 218–228.
[25] K. Kaneko, Progr. Theoret. Phys. 68 (1982) 669–672;
M.P. Kennedy, L.O. Chua, IEEE Trans. Circuits Syst. CAS-33 (1986) 974–980.
[26] E. Ott, Chaos in Dynamical Systems, second ed., Cambridge University Press, 1993, pp. 175–178.
[27] Note that fluctuations due to finite network size are on the order of $1/\sqrt{N} = 0.01$ for $N = 10{,}000$, which is many orders of magnitude larger than numerical round-off errors.
[28] H.E. Nusse, J.A. Yorke, Physica D 90 (1996) 242–261;
L. Poon, J. Campos, E. Ott, C. Grebogi, Internat. J. Bifur. Chaos 06 (1996) 251–265.
[29] The system is technically a non-autonomous system so that there are no equilibrium points. The saddle-like point seems to correspond to the saddle point for the frozen network with $\eta = \eta_0$.
[30] E.C.-Y. Ho, M. Strüber, M. Bartos, L. Zhang, F.K. Skinner, J. Neurosci. 32 (2012) 9931–9946.
[31] A. Wagemakers, E. Barreto, M.A.F. Sanjuán, P. So, in preparation.
[32] H. Daido, Physica D 91 (1996) 24–66.

Please cite this article in press as: P. So, et al., Networks of theta neurons with time-varying excitability: Macroscopic chaos, multistability, and final-state uncertainty, Physica D (2013), http://dx.doi.org/10.1016/j.physd.2013.04.009